Journal of Applied Physics

The search for the most conductive metal for narrow interconnect lines

Cite as: J. Appl. Phys. **127**, 050901 (2020); https://doi.org/10.1063/1.5133671
Submitted: 29 October 2019 • Accepted: 22 December 2019 • Published Online: 03 February 2020

Daniel Gall

AIP Publishing

Journal of Applied Physics PERSPECTIVE scitation.org/journal/jap

The search for the most conductive metal for narrow interconnect lines

Cite as: J. Appl. Phys. **127**, 050901 (2020); doi: 10.1063/1.5133671
Submitted: 29 October 2019 · Accepted: 22 December 2019 ·
Published Online: 3 February 2020

Daniel Gall

AFFILIATIONS

Department of Materials Science and Engineering, Rensselaer Polytechnic Institute, Troy, New York 12180, USA

ABSTRACT

A major challenge for the continued downscaling of integrated circuits is the resistivity increase of Cu interconnect lines with decreasing dimensions. Alternative metals have the potential to mitigate this resistivity bottleneck by either (a) facilitating specular electron interface scattering and negligible grain boundary reflection or (b) a low bulk mean free path that renders resistivity scaling negligible. Recent research suggests that specular electron scattering at the interface between the interconnect metal and the liner layer requires a low density of states at the interface and in the liner (i.e., an insulating liner) and either a smooth epitaxial metal-liner interface or only weak van der Waals bonding as typical for 2D liner materials. The grain boundary contribution to the room-temperature resistivity becomes negligible if the grain size is large (>200 nm or ten times the linewidth for wide or narrow conductors, respectively) or if the electron reflection coefficient is small due to low-energy boundaries and electronic state matching of neighboring grains. First-principles calculations provide a list of metals (Rh, Pt, Ir, Nb, Ru, Ni, etc.) with a small product of the bulk resistivity times the bulk electron mean free path $\rho_o \times \lambda$, which is an indicator for suppressed resistivity scaling. However, resistivity measurements on epitaxial layers indicate considerably larger experimental $\rho_o \times \lambda$ values for many metals, indicating the breakdown of the classical transport models at small (<10 nm) dimensions and suggesting that Ir is the most promising elemental metal for narrow high-conductivity interconnects, followed by Ru and Rh.

I. INTRODUCTION

The continued downscaling of integrated circuits[1,2] causes a resistivity increase of Cu interconnect lines with decreasing dimensions,[3–6] limiting power efficiency and causing the interconnect delay to exceed the gate delay.[7] Electron scattering at surfaces and grain boundaries causes the resistivity of, for example, 10-nm-wide Cu interconnect lines to be approximately an order of magnitude larger than that of bulk Cu.[4,8] This motivates diverse research efforts to reduce diffuse scattering at the Cu-liner interface[9–12] and electron reflection at Cu grain boundaries[5,13–16] as well as the search for conductors that may replace Cu as an interconnect material at small dimensions.[17–26] The evaluation of Cu replacement options is challenging because (i) the resistivity size effect is due to both surface and grain boundary scattering that depend on a myriad of parameters including interface roughness,[27–31] orientation,[32,33] chemistry,[10,34,35] and grain boundary density,[6,36,37] structure,[13,16] and orientation distribution;[5,14,15,38,39] and (ii) the widely used classical models fail in predicting the resistivity increase for narrow metal lines.[31,39,40] In addition, processing constraints and reliability considerations[20,21,41] also strongly affect the choice of an interconnect metal solution. This is because seed layers (to facilitate deposition) and diffusion barrier and liner layers (to suppress time-dependent dielectric breakdown and electromigration and facilitate adhesion) can occupy a considerable fraction of the interconnect cross-sectional area. For example, the line resistance of a 10-nm half-pitch Cu line is increased by approximately a factor of 3 by these layers.[2,4,8,42] Thus, interconnect metals that do not require liner and/or barrier layers provide considerable conductance benefits.[19,23,43,44] Such trade-offs are illustrated, for example, by Intel's introduction of Co as an interconnect metal for the first two interconnect levels with ≤20 nm half-pitch in the 10-nm-technology node.[45] In that case, a 1.7× higher line resistance is tolerated for these local Co interconnects because of the higher electromigration resistance of Co and the lower vertical contact resistance (facilitated by the higher Ti-based barrier conductance) in comparison to Cu lines with TaN barriers.[45–47]

Research on the resistivity size effect in metals over the last few years can be divided into four different approaches and visions. (1) Considerable efforts focus on the evaluation of promising interconnect metal replacement options including Co[19,22,48–52] and Ru.[17,23,25,52–55] These studies quantify the resistance scaling[43] of

polycrystalline lines that often include realistic liner and barrier layers, are fabricated with processing methods that are transferrable to semiconductor manufacturing, and are tested for electromigration resistance[56,57] and time-dependent dielectric breakdown performance.[21,23,26] Thus, these studies demonstrate promise, feasibility, and performance of new interconnect solutions. (2) Other researchers focus on specific electron scattering mechanisms and quantify the effect of specific material interfaces,[11,12,24,34,35,58–63] grain boundaries,[5,6,13–15,38,39,64,65] and surface roughness[1,27–30,66–68] on the resistivity using both experimental and computational methods. The goal of these studies is to understand these scattering mechanisms and discover materials systems, structures, and chemistries that reduce diffuse electron scattering and therefore increase conductance. (3) Some studies quantify the resistivity scaling for specific metals by employing idealized materials systems with the goal to determine the electron mean free path,[24,42,51,69–71] which is the characteristic length scale of the resistivity size effect within classical transport models that account for both surface and grain boundary scattering. This includes transport measurements on epitaxial metal layers[10,32,55,70,72,73] or first-principles simulations using the bulk electronic structure without explicit electron scattering.[32,74,75] (4) Finally, researchers also develop new quantum mechanical models that overcome the limitations of the classical models by correctly accounting for quantization in the 1- or 2-dimensional conductors and coherent scattering at surfaces, grain boundaries, and in the bulk.[76–81] These models are general; that is, they are applicable to all metals and therefore require as input parameters the conductor geometry and its electronic structure. They are particularly important at small length scales (<10 nm), where the classical models completely fail.[40,76,81]

In this perspectives article, I would like to discuss the resistivity size effect and its underlying physical processes from a materials selection perspective. That is, I discuss structure and property requirements for interconnect metals and adjoining liner layers that minimize the size effect and therefore lead to a high conduction in the limit of narrow wires. The majority of the discussion uses classical and semiclassical transport descriptions because their accessible concepts can be directly translated into materials properties that control the resistivity size effect. However, I would like to caution the reader and emphasize here that resistivity predictions from classical transport models both quantitatively and qualitatively diverge from experimental results as well as from fully quantum mechanical descriptions particularly in the limit of a small conductor size, as discussed at various places in this article. Nevertheless, the starting points here are the classical models by Fuchs and Sondheimer (FS)[82,83] and Mayadas and Shatzkes (MS)[36,37] that predict the resistivity contributions due to electron scattering at external surfaces and grain boundaries, respectively. Within first-level approximations, these contributions are additive, as illustrated in Fig. 1, which shows that the resistivity ρ of a wire is the sum of the bulk resistivity ρ_o plus contributions from surface and grain boundary scattering. This figure also illustrates the structure of this article: I first discuss electron surface scattering including the surface scattering specularity p, which is within the FS model a purely phenomenological parameter. Secondly, I discuss grain boundary scattering and the corresponding phenomenological reflection coefficient R. Thirdly, I discuss the product of the bulk resistivity times the bulk mean free path $\rho_o \times \lambda$, which is a prefactor for both the surface and grain boundary resistivity contributions and is directly determined by the electronic structure of a specific metal.

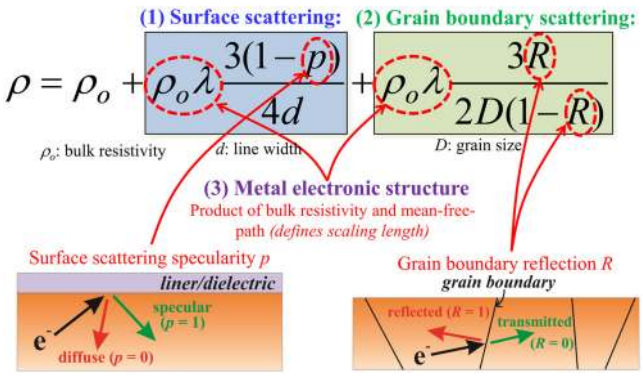

FIG. 1. Resistivity prediction from the approximate forms of the classical Fuchs and Sondheimer (FS)[82,83] and Mayadas and Shatzkes (MS)[36,37] models for a metal wire with a square cross section with width d and grain size D. The schematics illustrate the phenomenological parameters p and R for surface scattering specularity and grain boundary reflection. The product of the bulk resistivity times the bulk electron mean free path $\rho_o \times \lambda$ is the key contribution from the electronic structure.

II. ELECTRON SURFACE SCATTERING

Electron scattering at the interface between the conducting metal and the liner layer is one of the primary reasons for the interconnect resistivity increase with decreasing linewidth d. The classical Fuchs-Sondheimer model[82,83] uses a phenomenological specularity parameter p to distinguish between diffuse ($p = 0$) and specular ($p = 1$) surface scattering, as illustrated in Fig. 1. Diffuse scattering causes a randomization of the electron momentum. In contrast, during a specular scattering event, the momentum component parallel to the surface is retained. Therefore, specular scattering causes *no* resistivity increase and is desired to achieve high-conductivity interconnect lines. Figure 2(a) illustrates the specular surface scattering in a semiclassical picture. Here, the plane wave of an electron approaches the surface and excites an array of circular waves originating from surface sites that constructively interfere to form a reflected plane wave, analogous to the reflection of light from a mirror. Such reflection corresponds to specular scattering. Two key requirements for specular interface scattering have been determined from both experimental and computational research studies over the last approximately 5–10 years:

(a) *Interface roughness*: The interface needs to be atomically smooth. This is because electrons have a typical Fermi-wavelength on the order of 1 Å such that even atomic scale roughness results in destructive interference of reflected

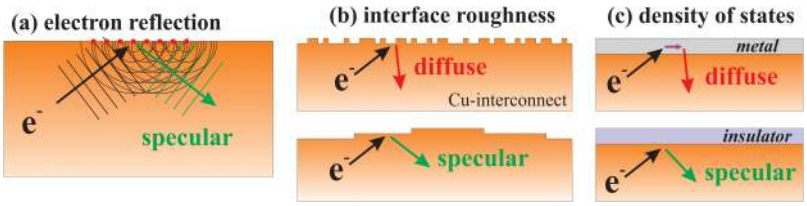

FIG. 2. Schematics illustrating that specular electron surface scattering (a) is the result of constructive interference of reflected waves, (b) requires atomically smooth surface terraces, and (c) is facilitated by an insulating liner with a negligible density of states.

waves and therefore causes diffuse surface scattering and a corresponding resistivity increase.[81] This requirement is most critical over short lateral length scales over which the electron wave is coherent. It can be relaxed over longer length scales, as illustrated in Fig. 2(b), which is based on reported mostly specular electron scattering at atomically smooth terraces even in the presence of some roughness.[11,84] I note that the interface roughness can also cause a resistance increase that is independent of the scattering specularity but is due to a varying conductor thickness[85] or electronic structure,[78,86,87] or reflection from step edges.[27] However, here I discuss the effect of interface roughness as it disturbs the flat potential step at the conductor-liner interface and leads to diffuse electron scattering.[29] This effect is similar to the adsorption of oxygen on an atomically smooth Cu surface, which disturbs the flat surface potential to cause effectively a roughening of the conducting Cu and a transition from specular to diffuse surface scattering.[11,34] Similarly, other adatoms including Ta and Ti on Cu surfaces also lead to diffuse electron scattering.[10,12]

(b) *Interface density of states*: Electrons that approach the interface and scatter into localized states in a conductive liner return to the Cu line with a random momentum, effectively resulting in diffuse scattering, as illustrated in Fig. 2(c). In contrast, insulating liners that have a negligible density of states at the Fermi-level $N(E_f)$ as well as a negligible interfacial $N(E_f)$ suppress this scattering mechanism, facilitating specular scattering and a correspondingly high Cu conductivity. This has been demonstrated experimentally using *in situ* transport measurements on epitaxial Cu(001) layers that were coated with metallic or insulating cap layers. More specifically, the addition of two monolayers (MLs) of Al or four MLs of Ti on Cu causes a transition from specular to diffuse electron surface scattering.[12,88] However, subsequent oxidation of the cap layers to form insulating oxides results in a resistivity decrease due to specular scattering at the interface between Cu and the surface oxides,[88] facilitated by the negligible surface $N(E_f)$.[12] I note here that direct oxidation of the Cu surface does not yield the same resistivity reduction,[34] because the interface between Cu and the Cu-oxide is not atomically smooth, resulting in diffuse scattering and a resistivity increase as discussed above. Similarly, even an atomically smooth interface between a metallic conductor and an insulating liner can exhibit localized interface states that the electrons scatter into. Thus, specular electron scattering at the metal-liner interface requires an insulating liner that also does not disturb the flat metal surface. This may be achieved with an epitaxial metal-liner interface or only weak van der Waals bonding of, for example, a 2D liner material.[59,60,62,89]

III. GRAIN BOUNDARY SCATTERING

Grain boundary scattering contributes to the resistivity size effect. This is because the grain size in microscopic conductors typically scales with the conductor size, such that narrow wires have small grains and correspondingly a large grain boundary density that leads to considerable electron scattering. According to the expression in Fig. 1, the resistivity contribution from grain boundary scattering is inversely proportional to the grain size D and increases with the phenomenological electron reflection parameter R that is defined by the probability of an electron to be backscattered by a grain boundary. Thus, there are two options to suppress the resistivity contribution from grain boundary scattering:

(a) *Increase the grain size D*. If the grain size is much larger than the bulk electron mean free path, then electron scattering at grain boundaries is negligible in comparison to electron-phonon scattering. More specifically, the resistivity contribution from grain boundaries becomes negligible (<10%) if the grain size exceeds 200 nm for a typical metal with $\lambda = 30$ nm and $R = 30\%$. Alternatively, for narrow conductors, grain boundary scattering is also negligible if the grain size is much larger than the linewidth. Its contribution to the resistivity is <10% if D is ten times larger than the width d, for a typical square wire with diffuse surface scattering. Thus, in summary, the resistivity contribution from grain boundary scattering in a typical metal becomes approximately negligible (<10%) if either the grain size is >200 nm or the grain size is ten times larger than the wire width.

(b) *Reduce the reflection coefficient R*. The average R is determined experimentally by quantifying the grain size distribution and its effect on the resistivity, yielding, for example, $R = 0.25$–0.43 for Cu.[3,5,6,90,91] However, R varies strongly as a function of boundary geometry as demonstrated using conductive scanning probe methods that allow to measure the specific resistance γ_R of individual grain boundaries.[15,92] For example, the most conductive grain boundary in Cu is the Σ3 twin boundary, with $\gamma_R = (0.155\text{–}0.17) \times 10^{-12}\,\Omega\,\mathrm{cm}^2$[14,15,38,93] and a corresponding R of only 0.016.[14] In contrast, the specific resistance of random grain boundaries is approximately two orders of magnitudes larger: $\gamma_R = (19\text{–}29) \times 10^{-12}\,\Omega\,\mathrm{cm}^2$,[15,92] which corresponds to $R = 0.65$–0.75, while coherent boundaries exhibit intermediate values of $\gamma_R = (0.7\text{–}2.4) \times 10^{-12}\,\Omega\,\mathrm{cm}^2$ corresponding to $R = 0.08$–0.22.[14,94] This strong variability may add additional challenges to narrow interconnects as a high-resistance boundary that crosses an entire line effectively represents a bottleneck for electron transport. Alternatively, this variability can possibly also be exploited by processing the metal

to exhibit only low-resistance boundaries. The first of two requirements for low-resistance grain boundaries is a small or negligible potential variation at the boundary. Figure 3(a) illustrates that a high-symmetry (low-energy) grain boundary such as the Σ3 boundary in Cu causes a low potential variation and correspondingly a low electron reflection probability, while the random boundary in Fig. 3(b) exhibits a space charge due to unsaturated bonds that leads to a larger potential barrier and a correspondingly higher electron reflection coefficient, consistent with the reported increase in γ_R with increasing atomic displacements at the boundaries[94] and an increasing interfacial energy.[14] Therefore, one approach to reduce R is to adjust metal processing to favor low-energy boundaries or to employ charge compensating dopants that reduce the boundary potential variation [as illustrated in Fig. 3(c)] and has been predicted by first-principle methods to reduce the specific resistance by up to a factor of two for multiple dopants in Cu.[13] The second requirement for a low-resistance boundary is a good matching of the electron states near the Fermi surface in the two adjacent grains. More specifically, an electron impinging on a grain boundary with energy E and momentum $\boldsymbol{p}$ can traverse the boundary without scattering if there exists an empty state with the same E and $\boldsymbol{p}$ in the new grain. The relevant energy for transport is the Fermi energy E_f. Traversing a grain boundary corresponds to a crystal rotation and a corresponding rotation of the Fermi surface. Thus, the probability for scattering-free transmission increases as the Fermi surface becomes more spherical and/or the conductor exhibits high-symmetry boundaries or textured conductors where the Fermi surfaces of the two grains align. I note that high-symmetry boundaries simultaneously also tend to be low-energy boundaries, thus, satisfying also the first requirement for low-resistance grain boundaries. Figure 3(d) shows, as examples, plots of the Fermi surfaces of Cu and W. The surface for Cu is close to a sphere, and its Fermi velocity indicated by the coloring is nearly constant. Therefore, electron transmission across grain boundaries is more likely in Cu than in W that has a much more anisotropic Fermi surface. This has been demonstrated quantitatively using first-principles calculations on coherent Σ5, Σ9, Σ11, and Σ17 boundaries, predicting specific resistances that are approximately an order of magnitude lower for Cu[14,94] than bcc W,[95] or 2–5 times smaller for Cu than for fcc Pt, Rh, Ir, Pd, and Al.[39,94] In summary, the resistivity contribution from grain boundary scattering is minimized if the grain size is large or the majority of grains exhibit a small reflection coefficient. The latter has two requirements, namely, low-energy boundaries that may be facilitated by annealing sequences or boundary doping and electronic state matching that is facilitated by spherical Fermi surfaces and/or grain alignment (texturing) or high-symmetry boundaries.

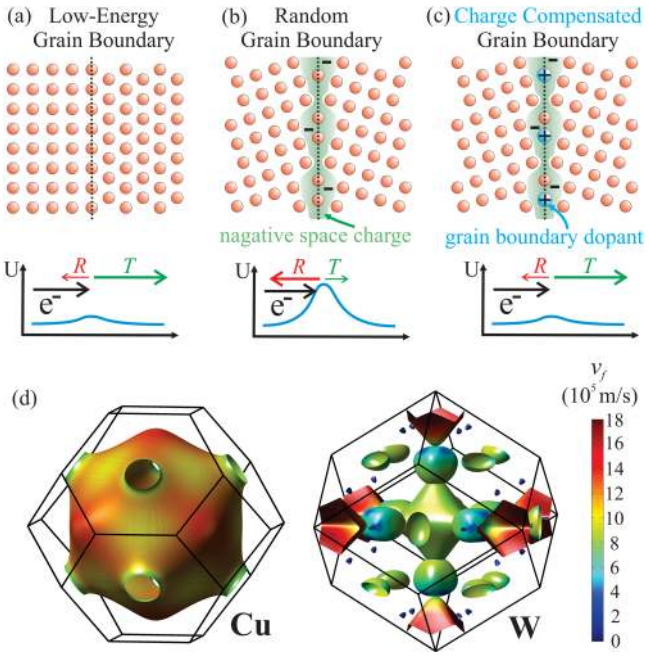

FIG. 3. Schematics illustrating (a) low-energy, (b) random, and (c) charge compensated grain boundaries. The variation in the potential U and the electron reflection probability R are small in (a) but large in (b) due to atomic displacements and charging near the random boundary. Dopants can compensate charging and reduce R [illustrated in (c)]. (d) Calculated Fermi surfaces of Cu and W, color coded according to their Fermi velocities v_f. The nearly spherical surface for Cu results in a lower grain boundary resistance than for W with an anisotropic Fermi surface.

IV. RESISTIVITY SCALING: METALS COMPARISON

The classical expression for the resistivity size effect in Fig. 1 shows that the resistivity contributions from electron scattering at external surfaces and grain boundaries are proportional to $\rho_o \times \lambda$. Therefore, in the limiting case of thin wires and/or small grain sizes, the wire resistivity becomes proportional to $\rho_o \times \lambda$ for any given fixed wire dimension and grain size distribution. Thus, the metal with the lowest product $\rho_o \times \lambda$ is expected to exhibit the highest conductivity in the limit of a small wire width. This argument neglects variations in the surface scattering specularity and grain boundary reflection coefficient that are expected to differ for different metals and also depend on the surface[10,11,30,34,35,88] and grain boundary[5,14–16,38] structure and chemistry, as discussed in Secs. II and III. In addition, these classical models tend to underestimate the resistivity for narrow (<10 nm) lines.[28,31,40,81,96] Nevertheless, minimizing the product $\rho_o \times \lambda$ is a useful starting point in the focused search for metals that form high-conductivity narrow wires.

The product $\rho_o \times \lambda$ is independent of temperature and electron scattering at impurities and crystalline defects since, within the classical transport description, electron scattering causes an increase in ρ_o and a corresponding decrease in λ. Therefore, $\rho_o \times \lambda$ can be directly calculated with numerical methods from the Fermi surface without the need to account for any electron-phonon interactions using[75]

$$\frac{1}{\lambda \rho_o} = \frac{e^2}{4\pi^3 \hbar} \sum_n \iint_{S_F^n} \frac{v_{t,n}^2(\boldsymbol{k})}{\boldsymbol{v}_n^2(\boldsymbol{k})} dS, \tag{1}$$

where the sum is over bands, the integration is over the Fermi surface S_F^n of band n, and the electron velocity along the transport direction $v_{t,n}(\boldsymbol{k})$ and the electron velocity vector $\boldsymbol{v}_n(\boldsymbol{k})$ are functions of the wave vector $\boldsymbol{k}$ for each band with index n. This expression is for the case of a constant $\boldsymbol{k}$-independent mean free path λ. Correspondingly, there is no need to explicitly calculate $\boldsymbol{v}_n(\boldsymbol{k})$ since the integral simplifies to a simple projection of the Fermi surface[97] and becomes exactly one-third of the area of the Fermi surface for materials with cubic symmetry.[18]

The $\rho_o \times \lambda$ product can be predicted using Eq. (1) and the Fermi surface that is obtained from first-principles. This has been done for the case of the 20 most conductive elemental metals[75] and also for other metals[24,42] and compounds.[74,98] Based on the above arguments, the metals with the lowest $\rho_o \times \lambda$ product are expected to exhibit the smallest resistivity size effect and should therefore be most conductive in the limit of narrow wires. Table I lists elemental metals with a calculated $\rho_o \times \lambda$ product that is smaller than that of Cu, suggesting at least 11 metals that have the potential to conduct better than Cu in the limit of narrow wires. The most promising Rh, Pt, and Ir have $\rho_o \times \lambda$ values that are approximately a factor of 2 smaller than for Cu.

Experimental quantification and direct comparison of the resistivity scaling in different metals are challenging due to the myriad of involved parameters including surface roughness, orientation, chemistry, and grain boundary density, structure, and orientation distribution, as discussed in Sec. I. Experiments that measure ρ as a function of linewidth or thin film thickness d typically find a resistivity increase that is approximately proportional to $1/d$ and fit the measured data with model expressions such as the one shown in Fig. 1, using measured values for d and D, while ρ_o is taken from the literature. However, this expression contains three unknown parameters, λ, p, and R, which cannot be independently determined as, e.g., an increase in R can be compensated by a decrease in λ or an increase in p, yielding diverse λ, p, and R sets that equally well describe experimental ρ vs d data. Our approach in attacking this challenge is to grow epitaxial metal layers such that confounding effects from grain boundary scattering is negligible, and the entire last term in the expression in Fig. 1 can be omitted. In addition, we use thin films rather than wires, because their thickness can be controlled and measured more accurately than the cross section of a wire, and the thin film surface roughness is typically much smoother than the line edge roughness of a wire. Thirdly, we compare the *in situ* and *ex situ* measured resistivity to quantify the effect of air exposure. This provides quantitative insight into the surface scattering specularity because, as discussed above, air exposure causes oxygen and/or water adsorption and a transition to completely diffuse surface scattering for many metals.

TABLE I. List of elemental metals that have a predicted $\rho_o \times \lambda$ product that is smaller than that of Cu.[42,75] The two listed values for hexagonal crystal structures are for transport perpendicular and parallel to the hexagonal axis.

	$\rho_o \times \lambda$ ($10^{-16}\,\Omega\,m^2$)
Rh	3.2
Pt	3.4
Ir	3.7
Ru	5.1/3.8
Nb	3.9
Ni	4.1
Ta	4.2
Os	6.4/4.3
Al	5.0
Fe	5.6
Mo	6.0
Cu	6.7

Figure 4 shows the *ex situ* measured room-temperature resistivity of epitaxial elemental metal layers as a function of their thickness d. The data are a summary of published and unpublished results from our group. The layers are deposited by sputtering on insulating single-crystal substrates including MgO(001), $Al_2O_3(0001)$, $Al_2O_3(11\bar{2}0)$, and $Al_2O_3(\bar{1}012)$. For each metal, the growth temperature and *in situ* annealing procedures have been optimized for maximum crystalline quality and minimum surface roughness, as quantified by x-ray diffraction, x-ray reflectivity, and transmission electron microscopy.[10–12,28,32,50,51,55,70,71,73,84,96,99] At large d, the plotted resistivity matches the known bulk values, with Ag and Cu having the lowest ρ_o while most other shown metals (Rh, Ir, W, Mo, Co, Ni, and Ru) have 3–5 times higher bulk resistivities. The resistivity increases with decreasing d for all metals due to electron surface scattering. However, this increase

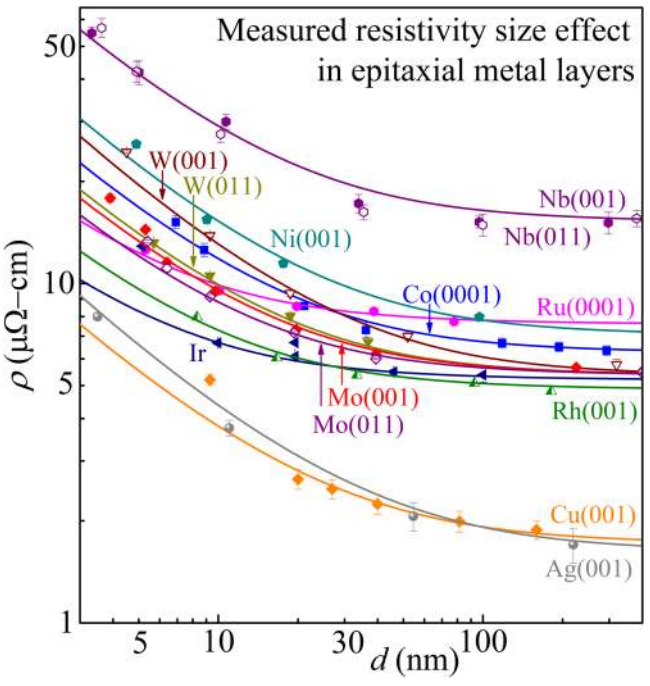

FIG. 4. Measured resistivity ρ vs thickness d of epitaxial metal layers. The data include unpublished results on Mo, Ir, and Rh as well as data from previous publications on Cu,[12] Ag,[70] W,[32] Ni,[71] Nb,[96] Ru,[55] and Co,[51] all from the Gall-group at RPI.

varies considerably for different metals, with Ir, Ru, and Rh showing particularly low resistivity increases, indicating a suppressed resistivity size effect due to a small bulk mean free path λ. This is quantified in the following and leads to promising high predicted conductivities for narrow lines of these metals, as discussed further below and in Fig. 5.

The lines through the data points in Fig. 4 are the result from curve fitting using the exact form of the Fuchs-Sondheimer model for thin films, which diverges for small d (below ~4 nm) from the approximate expression in Fig. 1[6] and also predicts a two times smaller resistivity contribution from scattering at two surfaces of a thin film (used here) vs four surfaces of a wire (Fig. 1). All curve-fitting is done using λ as a free fitting parameter and setting $p = 0$, corresponding to completely diffuse surface scattering. The latter assumption can be justified with the air exposure that is known to cause diffuse scattering for many metals.[11,12,34,51,71] However, more importantly, fixing $p = 0$ is a convenient choice to resolve the problem that the two parameters λ and p are strongly correlated and cannot be independently determined from curve fitting.[100] That is, with fixed $p = 0$, λ becomes the only and unique fitting parameter and effectively corresponds to a lower-bound for λ.[51,71] In the following, I refer to such a λ value as an "effective mean free path" λ_{eff}, which represents the fitting parameter that quantifies the resistivity scaling but may not necessarily match the bulk electron mean free path, because λ_{eff} is affected by a changing surface scattering specularity p and may therefore be a function of surface chemistry, structure, orientation, and roughness.

Table II is a list of the experimental λ_{eff} values, as determined by curve fitting of ρ vs d data in Fig. 4 from epitaxial metal layers. The table includes the predicted room-temperature λ values that are determined from the calculated Fermi surfaces using Eq. (1), as discussed above. Comparing the two columns indicates considerable differences between experiment and calculations. More specifically, there is reasonable agreement only for Cu and Ru. Most other metals show deviations between 25% and 45% (Ag, W, Co, Mo, Rh, and Ir) or even deviations by factors of 4, 9, and 9 for Ni, Ta, and Nb. The exact reason for these differences is still the focus of ongoing research. The following lists a few considerations and possible explanations:

TABLE II. The effective electron mean free path λ_{eff} determined experimentally from air-exposed epitaxial metal layers shown in Fig. 4 and the room-temperature bulk electron mean free path calculated from first-principles simulations[42,75] using reported ρ_o values at 293 K.[105] The two simulated values for hexagonal structures are for transport perpendicular and parallel to the hexagonal axis.

	Effective electron mean free path, λ_{eff} (nm)	
Metal	Experiment	Simulation
Cu(001)	39	39.9
Ag(001)	39	53.3
Ta(001)	28	3.21
Ni(001)	26	5.87
W(001)	33	19.1[a]
W(110)	19	11.2[a]
Nb(001)	20	2.36
Nb(110)	20	
Co(0001)	19	11.8/7.78
Mo(001)	17	11.2
Mo(110)	15	
Rh(001)	11	6.88
Ru(0001)	6.7	6.59/4.88
Ir	6.4	7.09

[a]The simulated values for W are specific for 001 and 110 oriented layers.[32]

(i) *Surface scattering specularity*: As discussed above, the experimental λ_{eff} listed in Table II are obtained assuming $p = 0$. Using $p > 0$ during data fitting would yield correspondingly larger λ_{eff} values and can explain the deviations for Ag and Ir. These are the only two metals for which λ_{eff} is smaller from experiment than from calculation. Both Ag and Ir surfaces are relatively inert and therefore expected to be more likely to exhibit specular electron scattering than many of the other listed metals. Thus, explaining the deviations for Ag and Ir with a $p > 0$ is quite plausible. On the other hand, this argument provides no explanation for the deviations for all other metals for which λ_{eff} from simulation is below that from experiment.

(ii) *Anisotropy*: The above calculations correctly account for the anisotropy in the Fermi surfaces and Fermi velocities but assume an isotropic electron-phonon scattering cross section, yielding a k-independent λ. The effect of the anisotropy in the Fermi velocity has been quantitatively evaluated for tungsten,[32] as also indicated in Table II that lists distinct λ_{eff} values for 001 and 110 oriented layers both from experiment and from simulation. The ratio of the listed 001 over 110 values is 1.7 from both experiment and simulation, indicating that the anisotropy of the Fermi velocity correctly predicts differences in the resistivity size effect with crystalline orientation. However, the values from the simulation for tungsten remain 41% below those from experiment. This deviation can in principle be explained with a k-dependent λ but requires for the case of W a carrier relaxation time that varies by more than an order of magnitude as a function of momentum direction.[32] Such a strong anisotropy in electron-phonon scattering is unexpected, based on reports on other metals,[101] suggesting that the anisotropy of electron-phonon scattering alone cannot explain the deviations in Table II.

(iii) *Surface roughness*: The effect of surface roughness on the electron scattering is conventionally included in the phenomenological specularity parameter p, which implies that the strongest contribution from surface roughness to the resistivity corresponds to completely diffuse ($p = 0$) surface scattering plus some minor geometrical effects.[85] However, some experimental[28] and computational[27] results suggest roughness effects that are stronger than what these conventional models predict,[82,85] leading to an unphysical $p < 0$ or alternatively λ_{eff} that is dependent on the experimental surface roughness and is larger than the true bulk mean free path. Thus, surface roughness could partially explain why experimental λ_{eff} values in Table II are larger than the calculated λ.

However, I note that curve fitting in Fig. 4 excludes outlier data points from the thinnest layers, such that exacerbated roughness effects at small thickness are already excluded from the reported λ_{eff} values.

(iv) *Crystalline defects*: Vacancies, impurities, and dislocations all cause an increase in the experimental resistivity and may cause λ_{eff} that is larger than the bulk mean free path if the defect density increases with decreasing layer thickness. The lattice mismatch between the substrate and the layers is relatively large for some of the heteroepitaxial metal layers presented in Fig. 4, causing strain fields from misfit dislocations that become more important with decreasing d and could therefore cause $\lambda_{eff} > \lambda$ for the data from Fig. 4.

(v) *Break-down of semiclassical transport models*: The classical Fuchs-Sondheimer (FS)[82,83] model employs the Boltzmann transport formalism where electron relaxation only occurs in the bulk and is quantified by λ, while diffuse surface scattering is accounted for by boundary conditions. The two key shortcomings of the FS model in the limit of narrow conductors are the assumptions that the electronic structure is bulk-like and that the surface scattering occurs exactly at the surface.[77] The latter becomes particularly evident in the limit of high-purity films at low temperature where the FS model predicts a vanishing resistivity for $\lambda \to \infty$. This is in direct contradiction to first-principles transport simulations[81] that are consistent with many reports that find the FS model to describe experimental data well for layer thicknesses that are comparable or larger than λ, but to consistently underestimate the measured resistivity for layers with $d < 20$ nm.[6,10–12,40,69,70,102,103] Correspondingly, data fitting of experimental ρ vs d data tends to overestimate λ, since the FS model underestimates the resistivity size effect at small d. This provides a possible explanation for the data in Table II, indicating that λ_{eff} from experiment is larger than the calculated bulk λ for many metals. I note that quantum mechanical models[76–80] that correctly account for the 2D transport in the plane of the thin film resolve these limitations of the FS model but do not provide a simple ρ vs d expression like the one in Fig. 1. As a result, the classical FS model is still widely used to describe experimental ρ vs d, yielding a single parameter λ_{eff} that quantifies the resistivity scaling, despite that λ_{eff} may not correspond to the actual physical bulk mean free path λ. Thus, in the following, I use the classical transport model and the experimental λ_{eff} from Table II to predict the resistivity scaling of polycrystalline lines. This is done with the knowledge that both the models have fundamental flaws and λ_{eff} is not necessarily an actual mean free path but simply a fitting parameter that quantifies the resistivity scaling for different metals.

Figure 5(a) shows the resistivity of wires with a square cross section as a function of width d. The curves are obtained using the measured λ_{eff} value from epitaxial layers and applying them to exact versions of the FS[82,83] and MS[36,37] models, assuming $p = 0$ in order to be consistent with the experimental determination of λ_{eff} discussed above and assuming an average grain size equal to the wire width ($D = d$) and an average grain boundary reflection coefficient $R = 0.4$. These latter values are typical for interconnect lines but can vary considerably depending on linewidth and processing conditions including deposition method and material composition and purity. Here, I simply use the same D and R values for all metals to provide a direct metal-to-metal comparison. Figure 5(a) indicates that three metals exhibit a lower ρ than copper for narrow polycrystalline wires. More specifically, Ru, Rh, and Ir have a resistivity below that of Cu for $d < 7$, 13, and 26 nm, respectively. This prediction excludes the effect of the metal microstructure and particularly the tendency for these high-melting-point metals to form small grains near the metal-liner interfaces of narrow lines, which result in nonuniform grain size distributions[104] and a resistance increase. In addition, the requirement for liner and/or diffusion barrier layers for certain metals can considerably affect the overall line resistance. To illustrate this effect, Fig. 5(b) is a plot of the line resistance vs half-pitch for interconnect lines with and without a 2-nm-thick liner layer for four relevant metals. The curves are

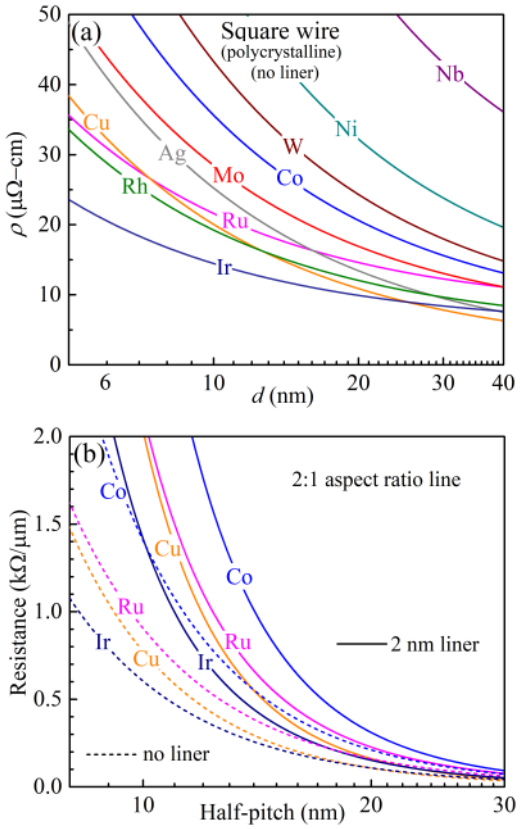

FIG. 5. (a) The resistivity ρ of polycrystalline square wires as a function of width d and (b) the resistance per micrometer of 2:1 aspect ratio interconnect lines vs half-pitch (i.e., width) with or without a 2-nm-thick liner, as labeled. The curves are predicted using the measured λ_{eff} values from Fig. 4, assuming a metal-independent grain boundary reflection coefficient $R = 0.4$ and grain sizes that are equal to the linewidth.

obtained using the experimental λ_{eff} and the classical transport models, as done for Fig. 5(a), but assuming a 2:1 height-to-width aspect ratio. The effect of the liner is determined simply based on the reduced cross-sectional area that is available for the interconnect metal, while neglecting effects that the liner may have on the metal microstructure and on the electron surface scattering specularity. For example, the conductor cross-sectional area without liner is $10 \times 20\,\text{nm}^2$ for a half-pitch of 10 nm but is reduced to $6 \times 18\,\text{nm}^2$ by a 2-nm-wide liner on both sidewalls and the bottom of the trench. This reduction in the cross-sectional area results, for example, in a quite substantial 2.6-fold resistance increase for a 10-nm-wide Cu line. Correspondingly, the dashed lines in Fig. 5(b) for the liner-free lines are well below the solid lines that account for a 2-nm-wide liner. This illustrates the strong impact that liners have on the resistance of narrow interconnect lines and suggests that metals that do not require liner/barrier layers may outperform metals with liners, even if the latter exhibit a lower resistivity size effect. In fact, comparing current liner options for Ru (0.3 nm), Co (1 nm), and Cu (2 nm)[9,23,53] indicates an advantage for Ru and also suggests that the Co line conductance may outperform Cu despite that Co exhibits a higher ρ for all d in Fig. 5(a).

V. CONCLUSIONS

The resistivity increase with decreasing width of interconnect lines is a major challenge for the continued downscaling of integrated circuits. This increase is due to electron scattering at surfaces and grain boundaries and can be limited using the following approaches:

(1) Electron surface scattering: The resistivity contribution from electron scattering at the metal-liner interface is suppressed if the scattering is specular. Requirements for specular scattering include (i) atomically smooth terraces at the metal-liner interface and (ii) an insulating liner that does not disturb the flat metal surface and, therefore, causes no localized interface states at the Fermi level. This may be achieved with an epitaxial metal-liner interface or a 2D liner material that forms no strong atomic bonds with the metal surface.
(2) Grain boundary scattering: The resistivity contribution from grain boundary scattering becomes negligible if (i) grains are large in comparison to the bulk electron mean free path or the linewidth. More specifically, if the average grain size is >200 nm or larger than 10× the linewidth (for lines with $d < 20$ nm), then the resistivity contribution from grain boundary scattering is expected to be <10%. Alternatively, grain boundary scattering is negligible if (ii) grain boundaries exhibit small electron reflection coefficients. This requires low-energy boundaries that may be facilitated by annealing sequences or boundary doping and electronic state matching that is facilitated by spherical Fermi surfaces and/or grain alignment (texturing) or high-symmetry boundaries.
(3) Metal choice: The classical transport models indicate that the metal with the smallest $\rho_o \times \lambda$ product exhibits the smallest resistivity in the limit of narrow wires. First-principles simulations provide a ranking of metals based on this criterion. However, resistivity measurements of epitaxial metal layers yield $\rho_o \times \lambda$ values that deviate considerably from the predictions, which may be due to a breakdown of the classical transport models for small dimensions or imperfections of the experimental samples including crystalline defects, surface roughness, or variations in the surface scattering specularity. Nevertheless, the experimentally measured mean free paths in combination with classical transport models provide predicted line resistance vs width curves, indicating that Ir, Rh, and Ru lines are expected to conduct better than Cu in the limit of narrow wires. In addition, the liner/barrier layer thickness is a critical parameter that strongly affects the line resistance of narrow interconnects. For example, the conductance of a 10 nm metal line that does not require a liner/barrier layer is expected to outperform the conductance of a metal that has a 2× lower resistivity but requires a 2-nm liner.

ACKNOWLEDGMENTS

This research is funded by the Semiconductor Research Corporation under Task 2881, the NY State Empire State Development's Division of Science, Technology and Innovation (NYSTAR) through Focus Center-NY–RPI Contract No. C150117, and the NSF under Grant Nos. 1740271 and 1712752. Computational resources were provided by the Center for Computational Innovations at RPI. The author thanks Atharv Jog for fruitful discussions and help with creating the figures.

REFERENCES

[1]D. Josell, S. H. Brongersma, and Z. Tőkei, Annu. Rev. Mater. Res. **39**, 231 (2009).
[2]International Roadmap Committee, . See http://www.itrs2.net for International Technology Roadmap for Semiconductors 2.0 (2015).
[3]J. J. Plombon, E. Andideh, V. M. Dubin, and J. Maiz, Appl. Phys. Lett. **89**, 113124 (2006).
[4]R. L. Graham, G. B. Alers, T. Mountsier, N. Shamma, S. Dhuey, S. Cabrini, R. H. Geiss, D. T. Read, and S. Peddeti, Appl. Phys. Lett. **96**, 042116 (2010).
[5]K. Barmak, A. Darbal, K. J. Ganesh, P. J. Ferreira, J. M. Rickman, T. Sun, B. Yao, A. P. Warren, and K. R. Coffey, J. Vac. Sci. Technol. A **32**, 061503 (2014).
[6]J. S. Chawla, F. Gstrein, K. P. O'Brien, J. S. Clarke, and D. Gall, Phys. Rev. B **84**, 235423 (2011).
[7]B. Q. Wu and A. Kumar, Appl. Phys. Rev. **1**, 011104 (2014).
[8]C. Y. Pan and A. Naeemi, IEEE Electron Device Lett. **35**, 250 (2014).
[9]M. H. v. d. Veen, N. Jourdan, V. V. Gonzalez, C. J. Wilson, N. Heylen, O. V. Pedreira, H. Struyf, K. Croes, J. Bömmels, and Z. Tőkei, in *IEEE International Interconnect Technology Conference/Advanced Metallization Conference (IITC/AMC)* (IEEE, 2016), p. 28.
[10]J. S. Chawla and D. Gall, Appl. Phys. Lett. **94**, 252101 (2009).
[11]P. Y. Zheng, R. P. Deng, and D. Gall, Appl. Phys. Lett. **105**, 131603 (2014).
[12]P. Y. Zheng, T. J. Zhou, and D. Gall, Semicond. Sci. Technol. **31**, 055005 (2016).
[13]M. Cesar, D. Gall, and H. Guo, Phys. Rev. Appl. **5**, 054018 (2016).
[14]M. Cesar, D. P. Liu, D. Gall, and H. Guo, Phys. Rev. Appl. **2**, 044007 (2014).
[15]T.-H. Kim, X. G. Zhang, D. M. Nicholson, B. M. Evans, N. S. Kulkarni, B. Radhakrishnan, E. A. Kenik, and A.-P. Li, Nano Lett. **10**, 3096 (2010).
[16]J. M. Rickman and K. Barmak, J. Appl. Phys. **114**, 133703 (2013).
[17]S. Dutta, S. Kundu, L. Wen, G. Jamieson, K. Croes, A. Gupta, J. Bömmels, C. J. Wilson, C. Adelmann, and Z. Tőkei, in *IEEE International Interconnect Technology Conference (IITC)* (IEEE, 2017), p. 1.
[18]D. Choi, C. S. Kim, D. Naveh, S. Chung, A. P. Warren, N. T. Nuhfer, M. F. Toney, K. R. Coffey, and K. Barmak, Phys. Rev. B **86**, 045432 (2012).
[19]V. Kamineni, M. Raymond, S. Siddiqui, F. Mont, S. Tsai, C. Niu, A. Labonte, C. Labelle, S. Fan, B. Peethala, P. Adusumilli, R. Patlolla, D. Priyadarshini, Y. Mignot, A. Carr, S. Pancharatnam, J. Shearer, C. Surisetty, J. Arnold,

D. Canaperi, B. Haran, H. Jagannathan, F. Chafik, and B. L. Herron, in *IEEE International Interconnect Technology Conference / Advanced Metallization Conference (IITC/AMC)* (IEEE, 2016), p. 105.
[20]J. S. Chawla, S. H. Sung, S. A. Bojarski, C. T. Carver, M. Chandhok, R. V. Chebiam, J. S. Clarke, M. Harmes, C. J. Jezewski, M. J. Kobrinski, B. J. Krist, M. Mayeh, R. Turkot, and H. J. Yoo, in *IEEE International Interconnect Technology Conference/Advanced Metallization Conference (IITC/AMC)* (IEEE, 2016), p. 63.
[21]Z. Xunyuan, H. Huai, R. Patlolla, W. Wei, F. W. Mont, L. Juntao, H. Chao-Kun, E. G. Liniger, P. S. McLaughlin, C. Labelle, E. T. Ryan, D. Canaperi, T. Spooner, G. Bonilla, and D. Edelstein, in *IEEE International Interconnect Technology Conference/Advanced Metallization Conference (IITC/AMC)* (IEEE, 2016), p. 31.
[22]J. Kelly, J. H. C. Chen, H. Huang, C. K. Hu, E. Liniger, R. Patlolla, B. Peethala, P. Adusumilli, H. Shobha, T. Nogami, T. Spooner, E. Huang, D. Edelstein, D. Canaperi, V. Kamineni, F. Mont, and S. Siddiqui, in *IEEE International Interconnect Technology Conference/Advanced Metallization Conference (IITC/AMC)* (IEEE, 2016), p. 40.
[23]W. Liang Gong, C. Adelmann, O. V. Pedreira, S. Dutta, M. Popovici, B. Briggs, N. Heylen, K. Vanstreels, C. J. Wilson, S. V. Elshocht, K. Croes, J. Bömmels, and Z. Tőkei, in *IEEE International Interconnect Technology Conference/Advanced Metallization Conference (IITC/AMC)* (IEEE, 2016), p. 34.
[24]S. Dutta, K. Sankaran, K. Moors, G. Pourtois, S. V. Elshocht, J. Bömmels, W. Vandervorst, Z. Tőkei, and C. Adelmann, J. Appl. Phys. **122**, 025107 (2017).
[25]X. Zhang, H. Huang, R. Patlolla, F. W. Mont, X. Lin, M. Raymond, C. Labelle, E. T. Ryan, D. Canaperi, T. E. Standaert, T. Spooner, G. Bonilla, and D. Edelstein, in *IEEE International Interconnect Technology Conference (IITC)* (IEEE, 2017), p. 1.
[26]C. K. Hu, J. Kelly, J. H. C. Chen, H. Huang, Y. Ostrovski, R. Patlolla, B. Peethala, P. Adusumilli, T. Spooner, L. M. Gignac, J. Bruley, C. Breslin, S. A. Cohen, G. Lian, M. Ali, R. Long, G. Hornicek, T. Kane, V. Kamineni, X. Zhang, F. Mont, and S. Siddiqui, in *IEEE International Interconnect Technology Conference (IITC)* (IEEE, 2017), p. 1.
[27]T. J. Zhou, P. Y. Zheng, S. C. Pandey, R. Sundararaman, and D. Gall, J. Appl. Phys. **123**, 155107 (2018).
[28]P. Y. Zheng, T. Zhou, B. J. Engler, J. S. Chawla, R. Hull, and D. Gall, J. Appl. Phys. **122**, 095304 (2017).
[29]Y. Q. Ke, F. Zahid, V. Timoshevskii, K. Xia, D. Gall, and H. Guo, Phys. Rev. B **79**, 155406 (2009).
[30]V. Timoshevskii, Y. Q. Ke, H. Guo, and D. Gall, J. Appl. Phys. **103**, 113705 (2008).
[31]P. T. Yukta, H. Andrew, F. S. Robert, M. L. Kim, K. Tung-Sheng, W. Gwo-Ching, and L. Toh-Ming, Nanotechnology **26**, 075704 (2015).
[32]P. Y. Zheng and D. Gall, J. Appl. Phys. **122**, 135301 (2017).
[33]D. Choi, M. Moneck, X. Liu, S. J. Oh, C. R. Kagan, K. R. Coffey, and K. Barmak, Sci. Rep. **3**, 2591 (2013).
[34]J. S. Chawla, F. Zahid, H. Guo, and D. Gall, Appl. Phys. Lett. **97**, 132106 (2010).
[35]F. Zahid, Y. Q. Ke, D. Gall, and H. Guo, Phys. Rev. B **81**, 045406 (2010).
[36]A. F. Mayadas and M. Shatzkes, Phys. Rev. B **1**, 1382 (1970).
[37]A. F. Mayadas, M. Shatzkes, and J. F. Janak, Appl. Phys. Lett. **14**, 345 (1969).
[38]L. Lu, Y. Shen, X. Chen, L. Qian, and K. Lu, Science **304**, 422 (2004).
[39]T. J. Zhou, N. A. Lanzillo, P. Bhosale, D. Gall, and R. Quon, AIP Adv. **8**, 055127 (2018).
[40]D. Choi, X. Liu, P. K. Schelling, K. R. Coffey, and K. Barmak, J. Appl. Phys. **115**, 104308 (2014).
[41]K. Croes, C. Adelmann, C. J. Wilson, H. Zahedmanesh, O. V. Pedreira, C. Wu, A. Lesniewska, H. Oprins, S. Beyne, I. Ciofi, D. Kocaay, M. Stucchi, Z. Tokei, and IEEE, in *IEEE International Electron Devices Meeting* (IEEE, 2018).
[42]D. Gall, in *IEEE International Interconnect Technology Conference (IITC)* (IEEE, 2018), p. 157.
[43]S. S. C. Fan, J. H. C. Chen, V. K. Kamineni, X. Zhang, M. Raymond, and C. Labelle, in *IEEE International Interconnect Technology Conference (IITC)* (IEEE, 2017), p. 1.
[44]T. Nogami, R. Patlolla, J. Kelly, B. Briggs, H. Huang, J. Demarest, J. Li, R. Hengstebeck, X. Zhang, G. Lian, B. Peethala, P. Bhosale, J. Maniscalco, H. Shobha, S. Nguyen, P. McLaughlin, T. Standaert, D. Canaperi, D. Edelstein, and V. Paruchuri, in *IEEE International Interconnect Technology Conference (IITC)* (IEEE, 2017), p. 1.
[45]A. Yeoh, A. Madhavan, N. Kybert, S. Anand, J. Shin, M. Asoro, S. Samarajeewa, J. Steigerwald, C. Ganpule, M. Buehler, A. Tripathi, V. Souw, M. Haran, S. Nigam, V. Chikarmane, P. Yashar, T. Mulé, Y. Wu, K. Lee, M. Aykol, K. Marla, P. Sinha, S. Kirby, H. Hiramatsu, W. Han, M. Mori, M. Sharma, H. Jeedigunta, M. Sprinkle, C. Pelto, M. Tanniru, G. Leatherman, K. Fischer, I. Post, and C. Auth, in *IEEE International Interconnect Technology Conference (IITC)* (IEEE, 2018), p. 144.
[46]F. W. Mont, X. Zhang, W. Wang, J. J. Kelly, T. E. Standaert, R. Quon, and E. T. Ryan, in *IEEE International Interconnect Technology Conference (IITC)* (IEEE, 2017), p. 1.
[47]G. Hegde, R. C. Bowen, and H. Simka, in *IEEE International Interconnect Technology Conference (IITC)* (IEEE, 2018), p. 163.
[48]J. Gu, D. Zhao, M. Kamon, D. M. Fried, G. Harm, and T. Mountsier, in *IEEE International Interconnect Technology Conference (IITC)* (IEEE, 2018), p. 7.
[49]J. Kelly, V. Kamineni, X. Lin, A. Pacquette, M. Hopstaken, Y. Liang, H. Amanapu, B. Peethala, L. Jiang, J. Demarest, H. Shobha, M. Raymond, and B. Haran, J. Electrochem. Soc. **166**, D3100 (2018).
[50]E. Milosevic, S. Kerdsongpanya, and D. Gall, in *IEEE Nanotechnology Symposium (ANTS)* (IEEE, 2018), p. 1.
[51]E. Milosevic, S. Kerdsongpanya, M. E. McGahay, A. Zangiabadi, K. Barmak, and D. Gall, J. Appl. Phys. **125**, 245105 (2019).
[52]C. K. Hu, J. Kelly, H. Huang, K. Motoyama, H. Shobha, Y. Ostrovski, J. H. C. Chen, R. Patlolla, B. Peethala, P. Adusumilli, T. Spooner, R. Quon, L. M. Gignac, C. Breslin, G. Lian, M. Ali, J. Benedict, X. S. Lin, S. Smith, V. Kamineni, X. Zhang, F. Mont, S. Siddiqui, F. Baumann, and IEEE, in *IEEE International Reliability Physics Symposium* (IEEE, 2018).
[53]S. Dutta, K. Moors, M. Vandemaele, and C. Adelmann, IEEE Electron Device Lett. **39**, 268 (2018).
[54]D. Wan, S. Paolillo, N. Rassoul, B. K. Kotowska, V. Blanco, C. Adelmann, F. Lazzarino, M. Ercken, G. Murdoch, J. Bömmels, C. J. Wilson, and Z. Tökei, in *IEEE International Interconnect Technology Conference (IITC)* (IEEE, 2018), p. 10.
[55]E. Milosevic, S. Kerdsongpanya, A. Zangiabadi, K. Barmak, K. R. Coffey, and D. Gall, J. Appl. Phys. **124**, 165105 (2018).
[56]O. V. Pedreira, K. Croes, H. Zahedmanesh, K. Vandersmissen, M. H. v. d. Veen, V. V. Gonzalez, D. Dictus, L. Zhao, A. Kolies, and Z. Tőkei, in *IEEE International Interconnect Technology Conference (IITC)* (IEEE, 2018), p. 48.
[57]M. H. v. d. Veen, N. Heyler, O. V. Pedreira, I. Ciofi, S. Decoster, V. V. Gonzalez, N. Jourdan, H. Struyf, K. Croes, C. J. Wilson, and Z. Tőkei, in *IEEE International Interconnect Technology Conference (IITC)* (IEEE, 2018), p. 172.
[58]H. Huang, N. Lanzillo, T. E. Standaert, K. Motoyama, C. Yang, H. Shobha, J. F. Maniscalco, T. Nogami, J. Li, T. A. Spooner, and G. Bonilla, in *IEEE International Interconnect Technology Conference (IITC)* (IEEE, 2018), p. 13.
[59]L. Li, H. S. P. Wong, and IEEE, in *IEEE International Electron Devices Meeting* (IEEE, New York, 2018).
[60]R. Mehta, S. Chugh, and Z. Chen, Nanoscale **9**, 1827 (2017).
[61]C. L. Lo, M. Catalano, K. K. H. Smithe, L. H. Wang, S. J. Zhang, E. Pop, M. J. Kim, and Z. H. Chen, NPJ 2D Mater. Appl. **1**, 42 (2017).
[62]R. Mehta, S. Chugh, and Z. H. Chen, Nano Lett. **15**, 2024 (2015).
[63]N. A. Lanzillo, P. Bhosale, C. Lavoie, D. J. Dechene, R. R. Robison, and K. Choi, J. Phys. D Appl. Phys. **52**, 495302 (2019).
[64]G. Hegde, R. C. Bowen, and M. S. Rodder, Appl. Phys. Lett. **109**, 193106 (2016).
[65]C. Arenas, R. Henriquez, L. Moraga, E. Munoz, and R. C. Munoz, Appl. Surf. Sci. **329**, 184 (2015).

[66]M. Wislicenus, R. Liske, L. Gerlich, B. Vasilev, and A. Preusse, Microelectron. Eng. **137**, 11 (2015).
[67]R. C. Munoz, R. Finger, C. Arenas, G. Kremer, and L. Moraga, Phys. Rev. B **66**, 205401 (2002).
[68]R. C. Munoz, G. Vidal, M. Mulsow, J. G. Lisoni, C. Arenas, A. Concha, F. Mora, R. Espejo, G. Kremer, L. Moraga, R. Esparza, and P. Haberle, Phys. Rev. B **62**, 4686 (2000).
[69]J. S. Chawla, X. Y. Zhang, and D. Gall, J. Appl. Phys. **113**, 063704 (2013).
[70]J. S. Chawla and D. Gall, J. Appl. Phys. **111**, 043708 (2012).
[71]E. Milosevic, P. Zheng, and D. Gall, IEEE Trans. Electron Devices **66**, 4326 (2019).
[72]J. M. Purswani and D. Gall, Thin Solid Films **516**, 465 (2007).
[73]P. Zheng, B. D. Ozsdolay, and D. Gall, J. Vac. Sci. Technol. A **33**, 061505 (2015).
[74]C. Adelmann, K. Sankaran, S. Dutta, A. Gupta, S. Kundu, G. Jamieson, K. Moors, N. Pinna, I. Ciofi, S. V. Eishocht, J. Bömmels, G. Boccardi, C. J. Wilson, G. Pourtois, and Z. Tőkei, in *IEEE International Interconnect Technology Conference (IITC)* (IEEE, 2018), p. 154.
[75]D. Gall, J. Appl. Phys. **119**, 085101 (2016).
[76]R. C. Munoz and C. Arenas, Appl. Phys. Rev. **4**, 011102 (2017).
[77]Z. Tesanovic, M. V. Jaric, and S. Maekawa, Phys. Rev. Lett. **57**, 2760 (1986).
[78]N. Trivedi and N. W. Ashcroft, Phys. Rev. B **38**, 12298 (1988).
[79]D. Calecki, Phys. Rev. B **42**, 6906 (1990).
[80]L. Sheng, D. Y. Xing, and Z. D. Wang, Phys. Rev. B **51**, 7325 (1995).
[81]T. J. Zhou and D. Gall, Phys. Rev. B **97**, 165406 (2018).
[82]K. Fuchs, Math. Proc. Cambridge Philos. Soc. **34**, 100 (1938).
[83]E. H. Sondheimer, Adv. Phys. **1**, 1 (1952).
[84]J. M. Purswani and D. Gall, J. Appl. Phys. **104**, 044305 (2008).
[85]Y. Namba, Jpn. J. Appl. Phys. **9**, 1326 (1970).
[86]H. K. Song, K. Xia, and J. Xiao, Sci. China Phys. Mech. Astron. **61**, 107011 (2018).
[87]G. Fishman and D. Calecki, Phys. Rev. Lett. **62**, 1302 (1989).
[88]E. Milosevic and D. Gall, IEEE Trans. Electron Devices **66**, 2692 (2019).
[89]T. Shen, D. Valencia, Q. Wang, K.-C. Wang, M. Povolotskyi, M. J. Kim, G. Klimeck, Z. Chen, and J. Appenzeller, ACS Appl. Mater. Interfaces **11**, 28345 (2019).
[90]T. Sun, B. Yao, A. P. Warren, K. Barmak, M. F. Toney, R. E. Peale, and K. R. Coffey, Phys. Rev. B **81**, 155454 (2010).
[91]J. W. Lim, K. Mimura, and M. Isshiki, Appl. Surf. Sci. **217**, 95 (2003).
[92]Y. Kitaoka, T. Tono, S. Yoshimoto, T. Hirahara, S. Hasegawa, and T. Ohba, Appl. Phys. Lett. **95**, 052110 (2009).
[93]B. H. Zhou, Y. Xu, S. Wang, G. H. Zhou, and K. Xia, Solid State Commun. **150**, 1422 (2010).
[94]N. A. Lanzillo, J. Appl. Phys. **121**, 175104 (2017).
[95]N. A. Lanzillo, H. Dixit, E. Milosevic, C. Y. Niu, A. V. Carr, P. Oldiges, M. V. Raymond, J. Cho, T. E. Standaert, and V. K. Kamineni, J. Appl. Phys. **123**, 154303 (2018).
[96]E. Milosevic, S. Kerdsongpanya, M. E. McGahay, B. Wang, and D. Gall, IEEE Trans. Electron Devices **66**, 3473 (2019).
[97]K. M. Schep, P. J. Kelly, and G. E. W. Bauer, Phys. Rev. B **57**, 8907 (1998).
[98]L. H. Chen, D. Ando, Y. Sutou, D. Gall, and J. Koike, Appl. Phys. Lett. **113**, 183503 (2018).
[99]J. M. Purswani, T. Spila, and D. Gall, Thin Solid Films **515**, 1166 (2006).
[100]S. S. Ezzat, P. D. Mani, A. Khaniya, W. Kaden, D. Gall, K. Barmak, and K. R. Coffey, J. Vac. Sci. Technol. A **37**, 031516 (2019).
[101]P. Narang, R. Sundararaman, and H. A. Atwater, Nanophotonics **5**, 96 (2016).
[102]S. M. Rossnagel and T. S. Kuan, J. Vac. Sci. Technol. B **22**, 240 (2004).
[103]J. S. Chawla, X. Y. Zhang, and D. Gall, J. Appl. Phys. **110**, 043714 (2011).
[104]M. Treger, C. Witt, C. Cabral, C. Murray, J. Jordan-Sweet, R. Rosenberg, E. Eisenbraun, and I. C. Noyan, J. Appl. Phys. **113**, 214904 (2013).
[105]W. M. Haynes, *CRC Handbook of Chemistry and Physics*, 95th ed. (CRC Press, Boca Raton, FL, 2014).